Chemical Science

ROYAL SOCIETY OF CHEMISTRY

EDGE ARTICLE

View Article Online
View Journal | View Issue

Cite this: *Chem. Sci.*, 2025, **16**, 13486

All publication charges for this article have been paid for by the Royal Society of Chemistry

Mechanistic insights into spontaneous redispersion of ZnO onto TiO_2 in water-containing environments†

Conghui Liu,[ab] Rongtan Li,[b] Xiaohui Feng,[b] Yuting Sun,[b] Yamei Fan,[b] Jiaxin Li[b] and Qiang Fu *[b]

Received 1st March 2025
Accepted 20th June 2025

DOI: 10.1039/d5sc01637a

rsc.li/chemical-science

Water has a profound effect on the surface structure and catalytic performance of numerous heterogeneous catalysts. Understanding the mechanism of structural evolution in water-containing reaction atmospheres is essential for the rational design of catalysts with enhanced catalytic efficiency and stability. In this work, we have observed spontaneous redispersion of physically mixed ZnO particles onto TiO_2 surfaces in water-containing environments at room temperature. Water vapor at a pressure greater than 3.2 kPa is a prerequisite for the efficient ZnO redispersion, in which a water adlayer with a thickness of about three monolayers forms on the TiO_2 surface. Raising the sample temperature to 50 °C or rendering the TiO_2 surface hydrophobic prevents the formation of the water adlayer and thereby inhibits the ZnO redispersion. Solid-state nuclear magnetic resonance spectroscopy and *in situ* spectroscopic analyses confirm that the surface water adlayer serves as a migration channel for ZnO species. Moreover, ZnO achieves more rapid and complete redispersion in a liquid water environment. This structural regulation strategy increases the number of exposed active sites in the ZnO–TiO_2 catalyst, leading to enhanced catalytic activity in propane dehydrogenation.

Introduction

Solid catalysts frequently undergo structural modifications during both pretreatment and catalytic reactions.[1–5] Controlled structural evolution can generate new active structures and increase the number of active sites, thereby enhancing catalytic performance.[6–9] For example, Ag particles can redisperse into single atoms in O_2 at 400 °C, which exhibit improved activity in selective catalytic reduction of NO with C_3H_6.[10,11] In the propane dehydrogenation reaction at 550 °C, ZnO migrates and anchors on hydroxyl nests of the silicalite-1 support, forming a highly stable active structure.[12,13] However, uncontrollable changes, such as sintering,[14–16] over-oxidation,[17,18] phase transition,[19,20] and loss of active components,[21,22] typically degrade catalytic efficiency. Therefore, it is crucial to understand the effects of surrounding media on the structural evolution of catalysts in order to construct active structures and prevent deactivation of the operating catalysts.

Water, as one of the most ubiquitous substances, plays a significant role in the structural evolution of many catalysts.[23,24] For instance, introduction of H_2O vapor into O_2 at 400 °C can promote redispersion of Ag and Cu nanoparticles supported on Al_2O_3.[10,25] H_2O vapor can induce a stable strong metal–support interaction (SMSI) structure in the Au/TiO_2 catalyst at 600 °C, enhancing the catalyst stability in CO oxidation reaction.[26] In addition, H_2O vapor can alter the chemical state of catalysts during high-temperature catalytic reactions, thereby promoting or inhibiting the catalytic processes.[17,27,28] Even at room temperature (RT), water vapor can induce structural evolution of supported catalysts.[29,30] For example, exposing the Ni/h-AlN catalyst to moist air at RT results in hydrolysis of AlN and further forms an SMSI structure.[31] Pretreatment of the Pd/SiO_2 catalyst in air containing 10% H_2O leads to aggregation of Pd nanoparticles and catalyst deactivation during the formaldehyde oxidation reaction.[29] Liquid water medium may have even stronger structural regulation effect on many catalysts. The strong covalent metal–support interaction of Pt single-atom catalysts with $CoFe_2O_4$ can be modulated by a simple water-soaking treatment, improving the catalytic activity of methane combustion.[32] Additionally, Ag clusters can aggregate to form large particles through Ostwald ripening in liquid water.[33] Although the influence of water on the structural evolution of catalysts is frequently observed, the underlying mechanisms remain to be explored in more detail.

In this study, we investigate the water effect on ZnO redispersion onto TiO_2 at RT. The degree of ZnO redispersion increases with the water content in water-containing gaseous environments. Solid-state nuclear magnetic resonance

[a]School of Chemistry, Dalian University of Technology, Dalian 116024, China
[b]State Key Laboratory of Catalysis, Chinese Academy of Sciences, Dalian Institute of Chemical Physics, Dalian 116023, China. E-mail: qfu@dicp.ac.cn

† Electronic supplementary information (ESI) available. See DOI: https://doi.org/10.1039/d5sc01637a

spectroscopy (NMR) and diffuse reflectance infrared Fourier transform spectroscopy (DRIFTS) studies demonstrate that the formation of a water adlayer with around three monolayer (ML) thickness on the TiO_2 surface is necessary for efficient ZnO redispersion, which requires water vapor pressure higher than 3.2 kPa at RT. Increasing H_2O vapor partial pressure enhances the formation of a thicker water adlayer and accelerates the ZnO redispersion process, and the maximum redispersion rate is achieved in liquid water. Low treatment temperature and support surface hydrophilization facilitate the formation of a thicker water adlayer under the same conditions. In contrast, increasing the temperature causes the stronger evaporation of surface-adsorbed water, and the hydrophobic treatment of the support prevents the formation of the water adlayer, both of which inhibit ZnO redispersion. The water-induced redispersion significantly reduces the size of ZnO particles, presenting a new regeneration method for sintered supported catalysts and enhancing catalytic performance in propane dehydrogenation (PDH).

Experimental

Sample preparation

ZnO powder (Macklin) was physically mixed with anatase TiO_2 powder (Macklin) at a 1 : 20 mass ratio to prepare a 5 wt% ZnO–TiO_2 sample. The sample was then treated in a H_2O/O_2 atmosphere, and the obtained sample was denoted as ZnO–TiO_2–H_2O. Additionally, the ZnO–TiO_2 sample was immersed in liquid water and subsequently dried to obtain the sample designated as ZnO–TiO_2–Water. The same method was employed to deposit 5 wt% ZnO onto γ-Al_2O_3 and SiO_2 supports with comparable specific surface areas, yielding 5 wt% ZnO–Al_2O_3 and 5 wt% ZnO–SiO_2 catalysts. The corresponding samples after H_2O/O_2 treatment were designated as ZnO–Al_2O_3–H_2O and ZnO–SiO_2–H_2O.

Saturated H_2O vapor was introduced into O_2 through a bubbler, and the resulting gas was denoted as 3.2% H_2O/O_2, where 3.2% refers to the proportion of 3.2 kPa H_2O vapor in the atmosphere. The content of H_2O vapor in the atmosphere was adjusted by mixing dry and moist O_2 in varying proportions. The resulting gases were denoted as 0.3% H_2O/O_2 and 1.6% H_2O/O_2 according to the proportion of H_2O vapor in the atmosphere. Supersaturated H_2O vapor in O_2 was generated by heating the bubbler to 40 °C, which was denoted as 7.4% H_2O/O_2.

TiO_2 was immersed and stirred in ammonia solution with concentrations of 28%, 14% and 3%, respectively, at RT for 12 h and then dried to produce TiO_2 with varying degrees of hydrophilicity.[34] Commercial hydrophobized TiO_2 (Macklin) was modified with stearic acid. ZnO was loaded onto the modified TiO_2 by physically mixing, producing samples designated as ZnO-hydrophilic TiO_2 and ZnO-hydrophobic TiO_2, respectively.

Characterization

Scanning transmission electron microscopy (STEM) images were acquired using a JEM-F200 high-resolution scanning transmission electron microscope operated at 200 kV, which was equipped with an energy dispersive X-ray spectroscope (EDS) for elemental analysis. X-ray diffraction (XRD) patterns were recorded on Empyrean-100 and SmartLab diffractometers using a Cu Kα radiation source ($\lambda = 1.5406$ Å) at a scanning rate of 10–20° min^{-1}. The ZnO diffraction peak at 36.3° was used to assess the degree of ZnO redispersion by normalizing its intensity to the TiO_2 diffraction peak at 25.5° and recording it as I_{ZnO}/I_{TiO_2}.

X-ray photoelectron spectroscopy (XPS) analyses were conducted on a SPECS spectrometer with either an Al Kα source (1486.6 eV) or a Mg Kα source (1253.6 eV) operated at 300 W. *In situ* XPS experiments were performed on a laboratory-based SPECS near-ambient pressure XPS (NAP-XPS) system. ZnO–TiO_2 samples were heated to various temperatures in a 0.5 mbar H_2O atmosphere, and then spectra were collected. The binding energies were calibrated using the C 1s peak at 284.8 eV. The Zn 2p peak was used as an indicator of the ZnO redispersion state,[35,36] and its intensity was normalized to the Ti 3d peak and recorded as A_{Zn2p}/A_{Ti3d}.

Solid-state NMR experiments were conducted using Bruker Avance NEO 400 MHz and Bruker Avance III 600 MHz NMR spectrometers, which are both equipped with a 4 mm H-X double resonance magic angle spinning (MAS) NMR probe. Single-pulse ^1H MAS NMR spectra were acquired at a spinning rate of 8 kHz with a π/2 pulse length of 3.3 or 5 μs. The chemical shifts for ^1H were referenced to adamantane at 1.74 ppm. The hydrogen amount in the samples was determined using polydimethylsiloxane (PDMS) as an external standard.

DRIFTS analysis was performed with a VERTEX 80V full-band high-resolution infrared spectrometer. *In situ* experiments were conducted by heating the sample to 450 °C in Ar for 1 h to remove surface adsorbates, then cooling it to the target temperature and exposing it to air containing 1.2% H_2O until saturation was reached.

Catalytic activity tests

The propane dehydrogenation reaction was evaluated using a microreactor connected to an Agilent 8890 gas chromatograph. A 0.20 g catalyst with 5 wt% ZnO loading in a quartz tube was heated to 550 °C in N_2 and then exposed to the reaction gas at the same temperature. The feed gas consisted of 5 vol% C_3H_8, 5 vol% Ar, N_2 balance and the total flow rate was 20 mL min^{-1}. Weight hourly space velocity (WHSV) was 0.54 h^{-1}. The products were analyzed using an online gas chromatograph equipped with a thermal conductivity detector (TCD) and a hydrogen flame ionization detector (FID).

The propane conversion and propylene selectivity were calculated as follows:

$$C_3H_8 \text{ conversion} = \frac{C_3H_{8in}^{TCD} - C_3H_{8out}^{TCD}}{C_3H_{8in}^{TCD}} \times 100\%$$

$$C_xH_y \text{ selectivity} = \frac{C_xH_{yout}^{FID} \times f}{\sum C_xH_{yout}^{FID} \times f} \times 100\%$$

$$\text{C balance} = \frac{\sum C_x H_{y\text{out}}^{\text{FID}} \times f}{C_3H_{8\text{in}}^{\text{FID}} - C_3H_{8\text{out}}^{\text{FID}}} \times 100\%$$

Here, TCD and FID refer to the signal sources. C_xH_y represents all hydrocarbon species except C_3H_8, and the symbol f stands for the relative correction factor. The inlet concentration is obtained using an empty tube test.

When investigating the effect of space velocity, feed gases containing 0.5 vol%, 1 vol%, and 40 vol% C_3H_8 were introduced while maintaining a constant flow rate of 20 mL min^{-1}. The pre-oxidation treatment involved heating the sample to 550 °C at a ramp rate of 10 °C min^{-1} under a 40 mL min^{-1} O_2 flow, followed by purging with 100 mL min^{-1} N_2 for 10 min prior to switching to the reaction gas. For catalyst regeneration, the used catalyst was exposed to 40 mL min^{-1} O_2 at the reaction temperature of 550 °C for 10 min, after which the system was switched back to the reaction gas. During all gas switching procedures, a 100 mL min^{-1} N_2 purge was consistently applied for 10 min to prevent gas mixing. The reaction order of propane dehydrogenation with respect to propane was determined by analyzing the reaction kinetics under varying concentrations of propane in the feed gas. Additionally, the activation energies of the catalytic reaction were calculated for both pristine and water-treated catalysts by examining the temperature-dependent reaction profiles. All kinetic experiments were conducted under differential reaction conditions, maintaining C_3H_8 conversion below 10% to ensure kinetic control. The studies employed gas flow rates of 20 or 40 mL min^{-1}, with 2 vol%, 5 vol%, and 10 vol% C_3H_8 in the reactant gas.

Results and discussion

H_2O-mediated spontaneous redispersion of ZnO onto the TiO_2 surface

The ZnO–TiO_2 sample with 5 wt% ZnO loading was prepared by physically mixing ZnO powder with anatase TiO_2 powder. In the XRD pattern, the distinct diffraction peaks at 31.8°, 34.5°, and 36.3° corresponding to the (100), (002) and (101) crystal planes of ZnO (PDF#75-0576) confirm the presence of ZnO particles in the ZnO–TiO_2 sample (Fig. 1a). After treatment in a 3.2% H_2O/O_2 atmosphere at RT for 12 h (denoted as ZnO–TiO_2–H_2O), the characteristic ZnO diffraction peaks almost disappear while TiO_2 diffraction peaks still remain unchanged (Fig. 1a and S1a†), suggesting either reduction in the size or decrease in the number of ZnO particles. Raman spectra exhibit the absence of ZnO vibrational modes, while the characteristic bands of TiO_2 also remain unaffected by the vapor treatment (Fig. S1b†). XPS results demonstrate a significant increase in the intensity of the Zn $2p_{3/2}$ peak at 1021.8 eV (Fig. S1c†) and a 4.7-fold increase in the Zn 2p/Ti 3d peak area ratio for the ZnO–TiO_2–H_2O sample (Fig. 1b), indicating enhanced dispersion degree of ZnO after H_2O vapor treatment.[37] STEM and EDS mapping images further reveal that most ZnO particles with sizes of hundreds of nanometers in the ZnO–TiO_2 sample (Fig. 1c) are no longer observable after the H_2O vapor treatment (Fig. 1d). The homogeneous

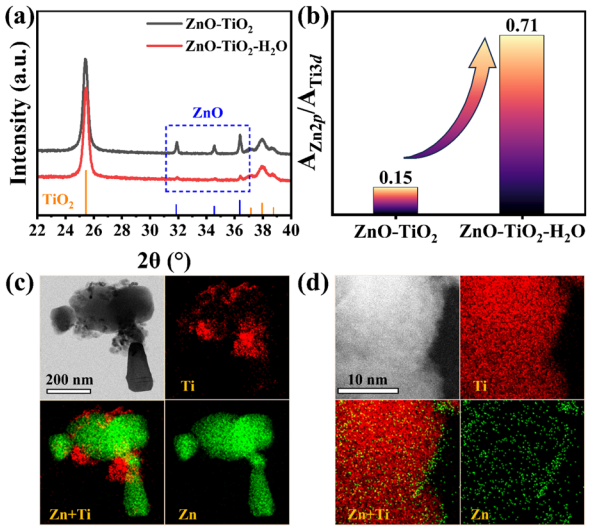

Fig. 1 Spontaneous redispersion of ZnO onto the TiO_2 surface. (a) XRD patterns of ZnO–TiO_2 and ZnO–TiO_2–H_2O samples. (b) Zn 2p/Ti 3d XPS peak area ratio of ZnO–TiO_2 and ZnO–TiO_2–H_2O samples. STEM and EDS mapping images of (c) ZnO–TiO_2 and (d) ZnO–TiO_2–H_2O samples.

distribution of Zn species across the TiO_2 support, as evidenced by EDS mapping images, suggests that the original large ZnO particles have redispersed into nanoclusters or nanolayers on the TiO_2 surface (Fig. 1d and S2†). These findings demonstrate that H_2O vapor treatment at ambient temperature can effectively induce spontaneous redispersion of ZnO onto TiO_2.

We further investigated ZnO redispersion onto different supports under water vapor treatment. For 5 wt% ZnO–Al_2O_3, the ZnO diffraction peaks weaken significantly yet remain detectable after the treatment (Fig. S3a†), while 5 wt% ZnO–SiO_2 shows negligible changes (Fig. S3b†). The observed variation in ZnO dispersity on different supports with comparable surface areas likely originates from the distinct ZnO–support interaction strength.[13,38]

Mechanism of H_2O-mediated ZnO redispersion

To investigate the effect of H_2O content on ZnO redispersion, ZnO–TiO_2 samples were treated in O_2 containing H_2O vapor with various partial pressures for 12 h and subsequently characterized using XRD and XPS. As shown in Fig. 2a, the intensity of ZnO diffraction peaks at 31.8°, 34.5°, and 36.3° remains unchanged for the samples treated in 0.3% and 1.6% H_2O/O_2, indicating that these H_2O partial pressures are insufficient to induce the spontaneous redispersion of ZnO. However, increasing the H_2O content to 2.3%, 3.2% or 7.4% leads to noticeable weakening of ZnO diffraction peaks under identical treatment conditions. Correspondingly, the Zn 2p/Ti 3d XPS peak area ratio of the sample treated in 1.6% H_2O/O_2 remains close to the initial value of 0.24. In contrast, the ratio increases by 1.9-fold in 2.3% H_2O/O_2, 3.0-fold in 3.2% H_2O/O_2 and by 3.7-fold in 7.4% H_2O/O_2 (Fig. 2b), indicating that the higher H_2O vapor partial pressures promote the stronger ZnO redispersion. Moreover, when the ZnO–TiO_2 sample is directly immersed in

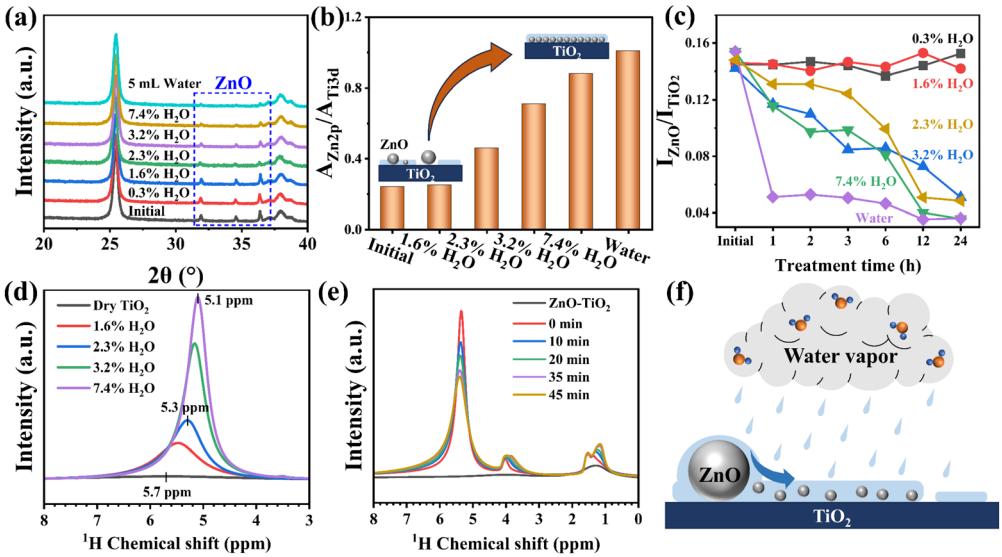

Fig. 2 Effect of H_2O content on ZnO redispersion. (a) XRD patterns of ZnO–TiO_2 treated in O_2 containing H_2O with various partial pressures for 12 h. (b) Zn 2p/Ti 3d XPS peak area ratios of ZnO–TiO_2 treated in O_2 containing H_2O with various partial pressures for 12 h. (c) ZnO diffraction peak intensity of ZnO–TiO_2 treated in O_2 containing H_2O with various partial pressures over time. (d) ^{1}H NMR spectra of TiO_2 treated in O_2 containing H_2O with various partial pressures for 3 h. (e) *In situ* ^{1}H NMR spectra of ZnO–TiO_2 after introducing 10 μL water without direct contact. (f) Schematic diagram of the formation of a water adlayer to promote ZnO redispersion onto TiO_2.

liquid water for 12 h, the ZnO diffraction peaks nearly disappear, accompanied by a 4.2-fold increase in the Zn 2p/Ti 3d ratio (Fig. 2a and b), suggesting that ZnO redisperses more completely in liquid water. The minimal leaching of Zn species (6.08 mg L^{-1} in filtrate) coupled with nearly constant Zn loading (3.76 wt%) in the ZnO–TiO_2 sample after water immersion demonstrates the absence of significant ZnO loss through dissolution. Complementary characterization by XRD and Raman further confirms that the structural integrity of TiO_2 remains unaltered in liquid water (Fig. S4†).

The relationship between the decrease rate of the ZnO diffraction peak intensity and the H_2O content in the gaseous atmosphere was assessed based on the XRD data. As shown in Fig. 2c, for the samples treated in 0.3% and 1.6% H_2O/O_2, the intensity of the ZnO diffraction peak at 36.3° remains unchanged over time. In contrast, the samples treated in 2.3%, 3.2% and 7.4% H_2O/O_2 show a rapid and continuous decrease in ZnO peak intensity. Furthermore, for the sample immersed in liquid water, the ZnO peak intensity experiences an abrupt reduction within the first hour, followed by a gradual decrease over time. These time-dependent profiles indicate that H_2O content modulates both the extent and rate of ZnO redispersion.

To explore the mechanism of water-promoting ZnO redispersion, ^{1}H NMR experiments were conducted on TiO_2 samples.[39] Fig. 2d shows a weak peak at 5.7 ppm in the ^{1}H NMR spectra of dry TiO_2, corresponding to hydrogen atoms in surface adsorbed water on TiO_2.[40,41] Upon treatment in O_2 with increasing H_2O contents for 3 h, the peak becomes more pronounced and shifts to the high-frequency region (5.1 ppm), indicating that the content of adsorbed water on TiO_2 increases with the H_2O partial pressure in the gaseous environment. Quantitative analysis using internal standards reveals that adsorbed water coverage increases from 0.2 ML on dry TiO_2 to 1.2 ML after 1.6% H_2O/O_2 treatment (Table S1†) while ZnO redispersion has not been observed under these conditions. The average water coverage on TiO_2 treated in 2.3%, 3.2% and 7.4% H_2O/O_2 reaches 1.7, 2.8 and 3.2 ML, respectively, in which cases ZnO redispersion starts to occur. This correlation suggests that a sufficient water adlayer thickness is required to facilitate the efficient migration and redispersion of ZnO. Previous molecular dynamics simulations demonstrate that the outermost water layer in the three layers of adsorbed water on the TiO_2 surface exhibits the highest mobility compared to inner layers,[42–45] potentially enabling ZnO transport through this hydrated interface.[33,46,47]

In situ solid-state NMR experiments were performed to observe the temporal evolution of water adlayer formation on TiO_2. Different volumes of liquid water were introduced into the closed rotor without contacting the TiO_2 sample, but allowing H_2O molecules to adsorb onto the TiO_2 surface through vapor phase transport. The initial spectrum shows a single peak at 5.6 ppm, corresponding to protons in the primary interfacial water (Fig. S5†), which is directly in contact with and strongly bound to TiO_2.[40] As the water volume increases, a new peak emerges at 4.9 ppm and becomes increasingly pronounced, which is attributed to mobile outer-layer water molecules interacting with the primary interfacial H_2O and OH groups through weaker hydrogen bonds.[45,48] The area ratio of these two peaks ($A_{4.9\ ppm}/A_{5.6\ ppm}$) increases from 0 to 2.0 as the water amount increases, demonstrating preferential accumulation of the outer-layer water. It is noteworthy that the ^{1}H NMR peak of outer-layer water (4.9 ppm) gradually weakens over time, while the peaks corresponding to interfacial water (5.6 ppm) and

hydroxyl groups (1.1 ppm) show an increase in intensity (Fig. S6†). This spectral evolution suggests continuous structural reorganization of the water adlayer, where outer-layer water transforms into interfacial water and hydroxyl groups.[40] The presence of merged signals in Fig. 2d reflects equilibrium between these dynamic processes, ultimately forming an interconnected hydrogen-bond network.[45]

In situ solid-state NMR experiments were performed on the ZnO–TiO_2 sample to observe the interaction between H_2O and ZnO. After introducing 10 μL water into the closed rotor without the direct contact between the water and the catalyst, the ^{1}H NMR spectrum shows the presence of a strong H_2O peak (5.4 ppm), a hydroxyl signal (1.1 ppm) and a peak at 3.9 ppm (Fig. 2e) identified as Zn–H species.[49–52] Over time, the water signal progressively decreases while both the hydroxyl and Zn–H signals increase (Fig. 2e), providing the direct evidence of ZnO-promoted water dissociation and the strong interaction between ZnO and H_2O. This ZnO redispersion process controlled by the water adlayer is illustrated in Fig. 2f.

Tuning ZnO redispersion by temperature or surface modification

As shown above, treatment in 3.2% H_2O/O_2 at RT for 12 h leads to the redispersion of ZnO onto TiO_2, as evidenced by the disappearance of ZnO diffraction peaks. However, when the treatment temperature increases from 20 to 50 °C under the identical 3.2% H_2O/O_2 conditions, the ZnO diffraction peaks exhibit progressively enhanced intensities (Fig. S7a†). At 50 °C and above, ZnO diffraction peaks remain almost unchanged (Fig. 3a). XPS results reveal that the Zn 2p/Ti 3d peak area ratio of the ZnO–TiO_2 sample increases 4.8-fold after treatment in 3.2% H_2O/O_2 at RT, but shows no significant change when treated at 50 °C (Fig. S7b†). These results demonstrate that elevated temperatures have an inhibitory effect on the spontaneous redispersion of ZnO in water-containing gaseous environments.

To probe this temperature-dependent phenomenon, the surface hydration states of TiO_2 were examined using solid-state NMR, DRIFTS and *in situ* XPS. The ^{1}H NMR spectrum of ZnO–TiO_2 treated in 3.2% H_2O/O_2 at 25 °C displays substantially stronger adsorbed water signals compared to the sample treated at 50 °C (Fig. 3b). Quantitative calculations indicate that the adsorbed water amount on TiO_2 in 3.2% H_2O/O_2 at 50 °C is limited to 0.2 ML. DRIFTS spectra further confirm this trend, where the H_2O peak at 3400 cm^{-1} (H–O stretching vibration peak of H_2O molecule[53]) shows negligible intensity variation between TiO_2 treated in H_2O/O_2 at 50 °C and TiO_2 without water treatment (Fig. 3c). In contrast, the TiO_2 treated in H_2O/O_2 at 25 °C exhibits markedly stronger absorption. *In situ* DRIFTS spectra shown in Fig. S7c† indicate that as the temperature decreases, the H_2O peak in the DRIFTS spectrum becomes stronger when the TiO_2 surface is saturated with adsorption in air containing 1.2% H_2O. *In situ* O 1s XPS spectra of the ZnO–TiO_2 sample show that exposure to 0.5 mbar H_2O atmosphere at RT increases both hydroxyl group content and adsorbed water signals (533.2 eV),[54,55] but the adsorbed water peak disappears upon heating to 50 °C (Fig. 3d). Collectively, the fact that high temperatures hinder ZnO redispersion is attributed to the suppressed formation of a water adlayer on the TiO_2 surface.

When ZnO–TiO_2 is immersed in liquid water at 90 °C for 3 h, XRD analysis shows complete disappearance of ZnO diffraction peaks (Fig. S7d†), demonstrating that elevated temperatures do

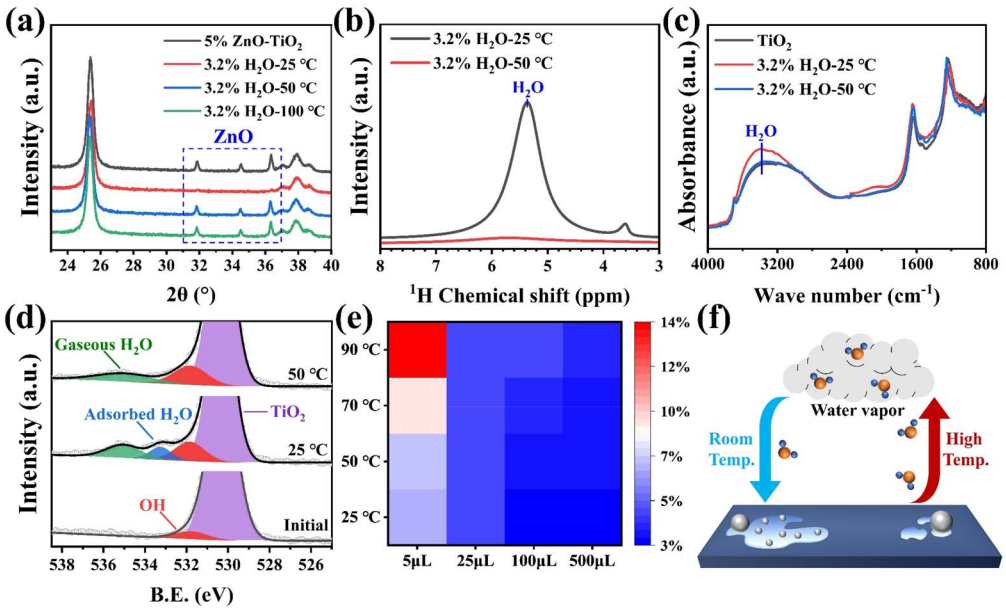

Fig. 3 Effect of temperature on ZnO redispersion. (a) XRD patterns of ZnO–TiO_2 before and after treatment in 3.2% H_2O/O_2 at different temperatures. (b) ^{1}H NMR and (c) DRIFTS spectra of ZnO–TiO_2 after treatment in 3.2% H_2O/O_2 at RT and 50 °C. (d) *In situ* O 1s XPS spectra of the ZnO–TiO_2 sample in a 0.5 mbar H_2O atmosphere at different temperatures. (e) Heat map of the diffraction peak intensity of ZnO at 36.3° in Fig. S5.† (f) Schematic diagram of the temperature-influenced ZnO redispersion process.

not inhibit ZnO redispersion in aqueous environments, in contrast to the gas-phase behavior. To investigate this contrast with gas-phase behavior, a 0.1 g ZnO–TiO_2 sample was placed in a 10 mL sealed bottle, and varying volumes of liquid water were introduced without direct contact with the sample. Then, these bottles were treated at different temperatures for 12 h and XRD analyses were conducted on the samples (Fig. S8†). The intensity variations of ZnO diffraction peaks at 36.3° are visualized as a heat map (Fig. 3e), which clearly demonstrates that elevated temperatures (50–90 °C) inhibit ZnO redispersion at low water volumes (5 μL), whereas this inhibitory effect diminishes when water quantity exceeds 25 μL. This temperature-dependent behavior primarily originates from different water evaporation rates at various temperatures (Table S2†). By correlating the average adsorbed water coverage with water evaporation behavior at different temperatures, we establish the temperature-dependent water requirements for ZnO redispersion in this system (Fig. S9†). These findings establish that temperature primarily modulates ZnO redispersion through its influence on adsorbed water availability under the evaporation–condensation equilibrium, rather than directly affecting reaction kinetics. The process of temperature-influenced ZnO redispersion is schematically illustrated in Fig. 3f.

Based on these findings, the possibility of surface chemical modification strategies to regulate ZnO redispersion was explored.[56–58] TiO_2 was pretreated with 28 wt% ammonia solution to enhance its hydrophilicity,[34] achieving a water contact angle of 10.1° *versus* 16.8° for untreated TiO_2 (Fig. 4a). When hydrophilic TiO_2 is employed for ZnO redispersion in 3.2% H_2O/O_2, ZnO diffraction peaks also significantly weaken, and XPS analysis demonstrates an increased Zn 2p/Ti 3d peak area ratio of 0.93 (Fig. 4b and c), exceeding the ratio of 0.71 observed with untreated TiO_2. Furthermore, a decrease in the concentration of used ammonia solution (14 wt% and 3 wt%) leads to reduction in the Zn 2p/Ti 3d ratio (0.82 and 0.77, respectively) after H_2O/O_2 treatment (Fig. 4c). In contrast, TiO_2 modified with stearic acid exhibits hydrophobic characteristics, having a water contact angle of 113.8° (Fig. 4a). XRD patterns reveal that ZnO diffraction peaks of the ZnO–hydrophobic TiO_2 sample remain unchanged after H_2O/O_2 treatment (Fig. 4d), indicating that ZnO cannot spontaneously redisperse onto hydrophobic TiO_2. The wetting property of the hydrophobic TiO_2 has been controlled by calcining at different temperatures, which is followed by ZnO loading and H_2O/O_2 treatment. The calcination at 100 or 200 °C has little effect on the XRD pattern and Zn 2p/Ti 3d ratio (Fig. 4d and e). After calcination at 300 °C, the ZnO diffraction peak intensity decreases but remains clearly detectable after H_2O/O_2 treatment, and the Zn 2p/Ti 3d ratio increases from 0.09 to 0.50 (Fig. 4d and e), indicating limited redispersion of ZnO. The results establish a direct correlation between TiO_2 hydrophilicity and ZnO redispersion efficiency.

Solid-state ^1H NMR was used to quantify the adsorbed water on the surface-modified TiO_2. After the treatment in 3.2% H_2O/O_2, hydrophilic TiO_2 retains 3.2 ML of adsorbed water, slightly

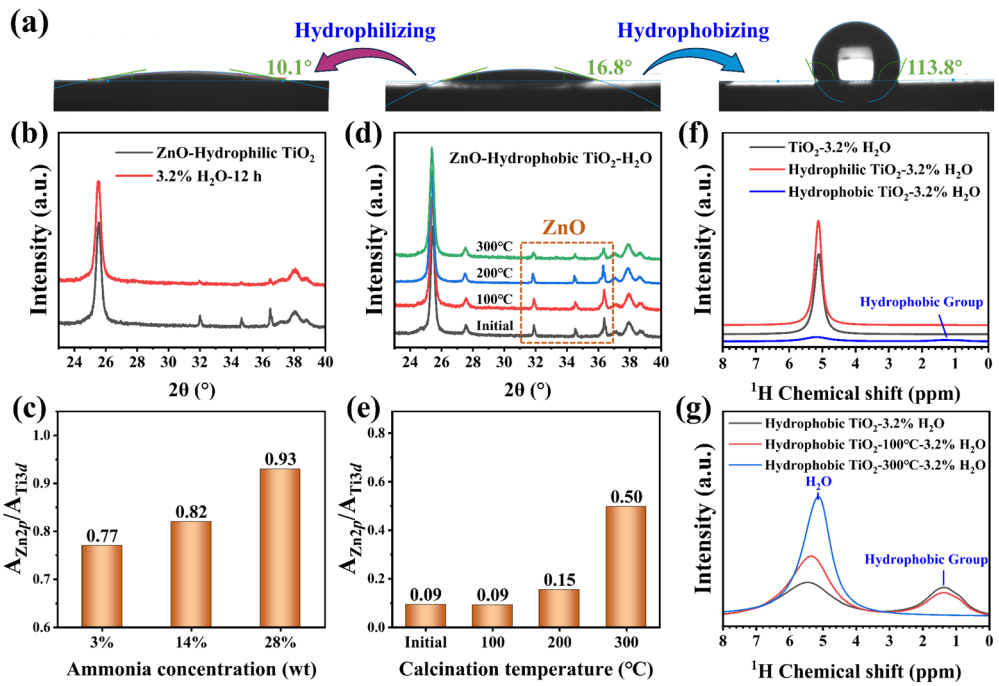

Fig. 4 Effect of support hydrophilicity and hydrophobicity on ZnO redispersion. (a) Contact angle measurement of water on fresh TiO_2, hydrophilic TiO_2 and hydrophobic TiO_2 samples. (b) XRD patterns of ZnO-hydrophilic TiO_2 before and after treatment in 3.2% H_2O/O_2. (c) Zn 2p/Ti 3d XPS peak area ratio of ZnO mixed with TiO_2 hydrophilized in ammonia solution with different concentrations and after H_2O/O_2 treatment. (d) XRD patterns and (e) Zn 2p/Ti 3d XPS peak area ratios of ZnO mixed with hydrophobic TiO_2 calcined at different temperatures and after treatment in 3.2% H_2O/O_2. (f) ^1H NMR spectra of TiO_2, hydrophilic TiO_2, and hydrophobic TiO_2 samples after treatment in 3.2% H_2O/O_2. (g) ^1H NMR spectra of hydrophobic TiO_2 calcined at different temperatures and after treatment in 3.2% H_2O/O_2.

exceeding 2.8 ML on untreated TiO_2. In contrast, hydrophobic TiO_2 exhibits a drastically reduced water adsorption capacity of 0.4 ML under identical conditions (Fig. 4f). ^{1}H NMR spectra further demonstrate that increasing the calcination temperature of hydrophobic TiO_2 progressively reduces the peak intensity of surface hydrophobic groups while enhancing the water adlayer peak after H_2O/O_2 treatment (Fig. 4g). Quantitative analysis reveals that hydrophobic TiO_2 calcined at 300 °C achieves only 0.9 ML of surface water coverage after H_2O/O_2 treatment. DRIFTS analysis corroborates these trends, where the O–H stretching vibration at 3400 cm^{-1} for hydrophobic TiO_2 remains less intense than that of untreated TiO_2 even after H_2O/O_2 treatment (Fig. S10†). These findings suggest that hydrophilic modification facilitates thicker water adlayer formation under the same conditions, thereby enhancing ZnO redispersion. Conversely, hydrophobic modification inhibits water adsorption, restricting water adlayer thickness below the critical threshold required for ZnO migration and redispersion. This systematic comparison conclusively demonstrates the indispensable role of outer-layer water in mediating ZnO redispersion.

Catalytic activity test

Propane dehydrogenation serves as a vital industrial process for propylene production. Zinc-based catalysts offer significant advantages in this process due to their low cost and environmental friendliness. To evaluate the impact of ZnO redispersion on catalytic activity, PDH activities of ZnO–TiO_2 samples were compared before and after H_2O treatment. As illustrated in Fig. 5a, the initial C_3H_8 conversion over ZnO–TiO_2–H_2O is significantly higher than that of ZnO–TiO_2, while C_3H_6 selectivity remains similar in a wide temperature range (Fig. S11†). Through kinetic analysis of PDH activity at varying temperatures and propane partial pressures, it is confirmed that the propane dehydrogenation reaction follows pseudo-first-order kinetics with respect to propane (Fig. S12†) and the activation energy of the PDH reaction remains essentially unchanged before and after water treatment of the catalyst (Fig. 5b). Therefore, the increase in C_3H_8 conversion of the ZnO–TiO_2 sample at 550 °C from 5.8% to 48.2% (8.3-fold enhancement) after water treatment mainly correlates with increased exposure of Zn–O active sites through the water-induced redispersion. ZnO–TiO_2–H_2O demonstrates notable catalytic performance for propane dehydrogenation among many Zn-based catalysts (Fig. 5c and Table S3†).[12,13,59–66] However, the catalyst rapidly deactivates due to ZnO consumption and carbon deposition under reductive conditions (Fig. S13a†). To improve stability, pre-oxidation (heating in 40 mL min^{-1} O_2) or regeneration (550 °C, 40 mL min^{-1} O_2, 10 min) is applied. Although initial conversion decreases from 48.2% to 26.8%, the ZnO–TiO_2–H_2O catalyst retains catalytic activity above 25% over 1 h operation with multiple regeneration cycles (Fig. 5d). Compared with the samples prepared by the impregnation method, the ZnO–TiO_2–H_2O catalyst consistently shows higher conversion and propylene space-time yield (STY) than 5% ZnO/TiO_2 (Fig. S13b†). In particular, after pre-oxidation or regeneration treatment and reaction for 40 min, the ZnO–TiO_2–H_2O catalyst retains a C_3H_8 conversion of ~28% with a propylene STY of 0.13 $g_{C_3H_6}$ h^{-1} g_{cat}^{-1}, outperforming the 5% ZnO/TiO_2 catalyst (~20% conversion, 0.09 $g_{C_3H_6}$ h^{-1} g_{cat}^{-1}).

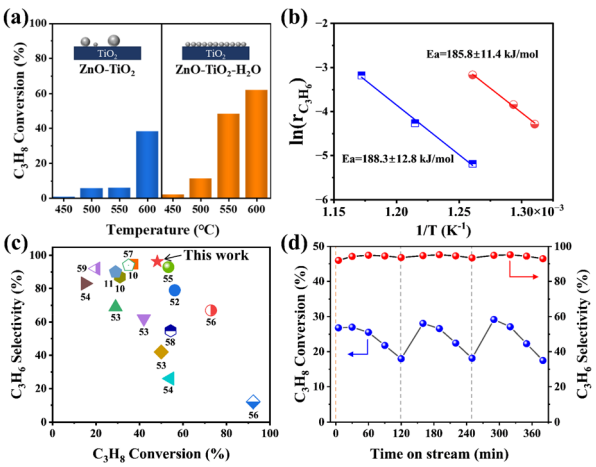

Fig. 5 Catalytic performance. (a) C_3H_8 conversion in the PDH reaction at different temperatures for ZnO–TiO_2 before and after H_2O treatment. Reaction conditions: 5 vol% C_3H_8, 5 vol% Ar, N_2 balance; WHSV = 0.54 h^{-1}. (b) Arrhenius plots for the calculation of the apparent activation energy of the propane dehydrogenation reaction over ZnO–TiO_2 catalysts. (c) Comparison of PDH performance of Zn-based catalysts in this work and other studies.[12,13,59–66] (d) Stability test of the ZnO–TiO_2–H_2O catalyst in the PDH reaction after pre-oxidation and regeneration (orange dashed line: pre-oxidation process, heating to 550 °C in 40 mL min^{-1} O_2; gray dashed line: regeneration process, treatment in 40 mL min^{-1} O_2 at 550 °C for 10 min).

Conclusions

This work establishes a water-mediated strategy for structural regulation of ZnO/TiO_2 catalysts. Through multiple characterization techniques, we demonstrate that ZnO spontaneously redisperses into nanoclusters or nanolayers on TiO_2 in the presence of water. The redispersion of ZnO is attributed to its strong interaction with TiO_2 and is influenced by the content of water present in the environment. Solid-state NMR analysis quantitatively correlates this phenomenon with water adlayer thickness, revealing that nearly 3 monolayers of adsorbed water generate sufficient outer-layer regions to enable efficient ZnO redispersion. Based on this understanding, increasing the temperature above 50 °C can limit the water adlayer to below 0.2 ML, and hydrophobically modifying TiO_2 also produces the adlayer with a coverage of 0.4 ML, both of which can completely inhibit the spontaneous redispersion of ZnO. The controlled regulation of ZnO size ultimately enhances the performance of the ZnO–TiO_2 catalyst in the propane dehydrogenation reaction, increasing C_3H_8 conversion by more than 8-fold and retaining propylene selectivity above 95%.

Data availability

The data that support the findings of this study are available within the article and the ESI.†

Author contributions

Q. F. conceived the project. C. L. and R. L. designed the studies. X. F. guided catalytic experiments. Y. S. performed NMR experiments. R. L. performed the *in situ* XPS experiment. C. L. performed other experiments. C. L., R. L., Y. F. and J. L. analyzed all the experimental data. C. L., R. L. and Q. F. wrote the manuscript. All authors interpreted the data and contributed to the preparation of the manuscript.

Conflicts of interest

There are no conflicts to declare.

Acknowledgements

This work was financially supported by the National Key R&D Program of China (2021YFA1502800, 2022YFA1504800 and 2022YFA1504500), National Natural Science Foundation of China (21825203, 22288201, 22332006 and 22321002), Fundamental Research Funds for the Central Universities (20720220009), Photon Science Center for Carbon Neutrality, and Dalian Innovation Support Plan for High Level Talents (2023RG002).

References

1 L. Piccolo, Restructuring effects of the chemical environment in metal nanocatalysis and single-atom catalysis, *Catal. Today*, 2021, **373**, 80–97.
2 Z.-P. Wu, S. Shan, S.-Q. Zang and C.-J. Zhong, Dynamic Core-Shell and Alloy Structures of Multimetallic Nanomaterials and Their Catalytic Synergies, *Acc. Chem. Res.*, 2020, **53**, 2913–2924.
3 S. Zhao, Y. Yang and Z. Tang, Insight into Structural Evolution, Active Sites, and Stability of Heterogeneous Electrocatalysts, *Angew. Chem., Int. Ed.*, 2022, **61**, e202110186.
4 B. Zhu, J. Meng, W. Yuan, X. Zhang, H. Yang, Y. Wang and Y. Gao, Reshaping of Metal Nanoparticles Under Reaction Conditions, *Angew. Chem., Int. Ed.*, 2019, **59**, 2171–2180.
5 W. Tan, S. Xie, X. Zhang, K. Ye, M. Almousawi, D. Kim, H. Yu, Y. Cai, H. Xi, L. Ma, S. N. Ehrlich, F. Gao, L. Dong and F. Liu, Fine-Tuning of Pt Dispersion on Al_2O_3 and Understanding the Nature of Active Pt Sites for Efficient CO and NH_3 Oxidation Reactions, *ACS Appl. Mater. Interfaces*, 2024, **16**, 454–466.
6 Z. W. Seh, J. Kibsgaard, C. F. Dickens, I. Chorkendorff, J. K. Nørskov and T. F. Jaramillo, Combining theory and experiment in electrocatalysis: Insights into materials design, *Science*, 2017, **355**, eaad4998.
7 W. Huang, A. C. Johnston-Peck, T. Wolter, W. D. Yang, L. Xu, J. Oh, B. A. Reeves, C. Zhou, M. E. Holtz, A. A. Herzing, A. M. Lindenberg, M. Mavrikakis and M. Cargnello, Steam-created grain boundaries for methane C-H activation in palladium catalysts, *Science*, 2021, **373**, 1518–1523.
8 M. Chen, B. Wu, J. Yang and N. Zheng, Small Adsorbate-Assisted Shape Control of Pd and Pt Nanocrystals, *Adv. Mater.*, 2012, **24**, 862–879.
9 B. Zhang, J. Yang, Y. Mu, X. Ji, Y. Cai, N. Jiang, S. Xie, Q. Qian, F. Liu, W. Tan and L. Dong, Fabrication of Highly Dispersed Ru Catalysts on CeO_2 for Efficient C_3H_6 Oxidation, *Environ. Sci. Technol.*, 2024, **58**, 19533–19544.
10 C. Liu, R. Li, F. Wang, K. Li, Y. Fan, R. Mu and Q. Fu, Water promoted structural evolution of Ag nanocatalysts supported on alumina, *Nano Res.*, 2023, **16**, 9107–9115.
11 F. Wang, J. Z. Ma, S. H. Xin, Q. Wang, J. Xu, C. B. Zhang, H. He and X. C. Zeng, Resolving the puzzle of single-atom silver dispersion on nanosized γ-Al_2O_3 surface for high catalytic performance, *Nat. Commun.*, 2020, **11**, 529.
12 D. Zhao, X. Tian, D. E. Doronkin, S. Han, V. A. Kondratenko, J. D. Grunwaldt, A. Perechodjuk, T. H. Vuong, J. Rabeah, R. Eckelt, U. Rodemerck, D. Linke, G. Jiang, H. Jiao and E. V. Kondratenko, In situ formation of ZnO_x species for efficient propane dehydrogenation, *Nature*, 2021, **599**, 234–238.
13 D. Zhao, K. Guo, S. Han, D. E. Doronkin, H. Lund, J. Li, J.-D. Grunwaldt, Z. Zhao, C. Xu, G. Jiang and E. V. Kondratenko, Controlling Reaction-Induced Loss of Active Sites in ZnO_x/Silicalite-1 for Durable Nonoxidative Propane Dehydrogenation, *ACS Catal.*, 2022, **12**, 4608–4617.
14 S. B. Duan, R. M. Wang and J. Y. Liu, Stability investigation of a high number density Pt_1/Fe_2O_3 single-atom catalyst under different gas environments by HAADF-STEM, *Nanotechnology*, 2018, **29**, 204002.
15 Y. Nishihata, J. Mizuki, T. Akao, H. Tanaka, M. Uenishi, M. Kimura, T. Okamoto and N. Hamada, Self-regeneration of a Pd-perovskite catalyst for automotive emissions control, *Nature*, 2002, **418**, 164–167.
16 J.-S. Lee and J.-H. Yu, Diffusion-Controlled Grain Growth in Liquid-Phase Sintering of W-Cu Nanocomposites, *Int. J. Mater. Res.*, 2001, **92**, 663–668.
17 J. Zhu, P. Wang, X. Zhang, G. Zhang, R. Li, W. Li, T. P. Senftle, W. Liu, J. Wang, Y. Wang, A. Zhang, Q. Fu, C. Song and X. Guo, Dynamic structural evolution of iron catalysts involving competitive oxidation and carburization during CO_2 hydrogenation, *Sci. Adv.*, 2022, **8**, eabm3629.
18 Y. Yazawa, N. Kagi, S.-i. Komai, A. Satsuma, Y. Murakami and T. Hattori, Kinetic study of support effect in the propane combustion over platinum catalyst, *Catal. Lett.*, 2001, **72**, 157–160.
19 G. Chen, R. Wang, W. Zhao, B. Kang, D. Gao, C. Li and J. Y. Lee, Effect of Ru crystal phase on the catalytic activity of hydrolytic dehydrogenation of ammonia borane, *J. Power Sources*, 2018, **396**, 148–154.
20 A. N. Pour and M. Housaindokht, Effects of metallic cobalt crystal phase on catalytic activity of cobalt catalysts supported on carbon nanotubes in Fischer-Tropsch synthesis, *Prog. React. Kinet. Mech.*, 2019, **44**, 316–323.
21 P. Gallezot, P. J. Cerino, B. Blanc, G. Flèche and P. Fuertes, Glucose hydrogenation on promoted raney-nickel catalysts, *J. Catal.*, 1994, **146**, 93–102.

22 M. Besson and P. Gallezot, Selective oxidation of alcohols and aldehydes on metal catalysts, *Catal. Today*, 2000, **57**, 127–141.

23 A. Goguet, R. Burch, Y. Chen, C. Hardacre, P. Hu, R. W. Joyner, F. C. Meunier, B. S. Mun, D. Thompsett and D. Tibiletti, Deactivation Mechanism of a $Au/CeZrO_4$ Catalyst During a Low-Temperature Water Gas Shift Reaction, *J. Phys. Chem. C*, 2007, **111**, 16927–16933.

24 D. Li, F. Xu, X. Tang, S. Dai, T. Pu, X. Liu, P. Tian, F. Xuan, Z. Xu, I. E. Wachs and M. Zhu, Induced activation of the commercial $Cu/ZnO/Al_2O_3$ catalyst for the steam reforming of methanol, *Nat. Catal.*, 2022, **5**, 99–108.

25 A. A. Liu, L. C. Liu, Y. Cao, J. M. Wang, R. Si, F. Gao and L. Dong, Controlling dynamic structural transformation of atomically dispersed CuO_x species and influence on their catalytic performances, *ACS Catal.*, 2019, **9**, 9840–9851.

26 H. Wang, X. Dong, Y. Hui, Y. Niu, B. Zhang, L. Liu, J. Cao, M. Yabushita, Y. Nakagawa, K. Tomishige, Y. Qin, L. Song, J. Xiao, L. Wang and F.-S. Xiao, Oxygen-Saturated Strong Metal-Support Interactions Triggered by Water on Titania Supported Catalysts, *Adv. Funct. Mater.*, 2023, **33**, 2304303.

27 J. Dong, Q. Fu, H. Li, J. Xiao, B. Yang, B. Zhang, Y. Bai, T. Song, R. Zhang, L. Gao, J. Cai, H. Zhang, Z. Liu and X. Bao, Reaction-Induced strong metal-support interactions between metals and inert boron nitride nanosheets, *J. Am. Chem. Soc.*, 2020, **142**, 17167–17174.

28 M. Wang, P. Wang, G. Zhang, Z. Cheng, M. Zhang, Y. Liu, R. Li, J. Zhu, J. Wang, K. Bian, Y. Liu, F. Ding, T. P. Senftle, X. Nie, Q. Fu, C. Song and X. Guo, Stabilizing Co_2C with H_2O and K promoter for CO_2 hydrogenation to C_{2+} hydrocarbons, *Sci. Adv.*, 2023, **9**, eadg0167.

29 C. Wang, J. Wang, X. Liu, Y. Li, C. Zhang, Y. Zheng and W. Shan, Abnormal inhibiting effect of H_2O on Pd/SiO_2 and $Na\text{-}Pd/SiO_2$ catalysts for HCHO oxidation, *Catal. Sci. Technol.*, 2023, **13**, 6409–6414.

30 Y. Fan, R. Li, B. Wang, X. Feng, X. Du, C. Liu, F. Wang, C. Liu, C. Dong, Y. Ning, R. Mu and Q. Fu, Water-assisted oxidative redispersion of Cu particles through formation of Cu hydroxide at room temperature, *Nat. Commun.*, 2024, **15**, 3046.

31 S. Li, Y. Fu, W. Kong, B. Pan, C. Yuan, F. Cai, H. Zhu, J. Zhang and Y. Sun, Dually confined Ni nanoparticles by room-temperature degradation of AlN for dry reforming of methane, *Appl. Catal., B*, 2020, **277**, 118921.

32 J. Yang, Y. Huang, H. Qi, C. Zeng, Q. Jiang, Y. Cui, Y. Su, X. Du, X. Pan, X. Liu, W. Li, B. Qiao, A. Wang and T. Zhang, Modulating the strong metal-support interaction of single-atom catalysts via vicinal structure decoration, *Nat. Commun.*, 2022, **13**, 4244.

33 C. Liu, R. Li, Y. Fan, S. Li, X. Feng, L. Feng, Y. Ning and Q. Fu, Liquid-mediated Ostwald ripening of Ag-based clusters supported on oxides, *Nano Res.*, 2024, **17**, 4971–4978.

34 Q. Kang, G. Li, Z. Li, Y. Tian and C. Wang, Surface co-hydrophilization via ammonia inorganic strategy for low-temperature Cu/SiO_2 hybrid bonding, *J. Mater. Sci. Technol.*, 2023, **149**, 161–166.

35 A. M. Tarditi, M. F. Mori and L. M. Cornaglia, Determination of the Metal Dispersion of Supported Catalysts Using XPS, *Top. Catal.*, 2019, **62**, 822–837.

36 Z. D. Davis and B. J. Tatarchuk, Understanding the dispersion of Ag on high surface area TiO_2 supports using XPS intensity ratios, *Appl. Surf. Sci.*, 2015, **353**, 679–685.

37 R. Li, X. Xu, B. Zhu, X. Y. Li, Y. Ning, R. Mu, P. Du, M. Li, H. Wang, J. Liang, Y. Chen, Y. Gao, B. Yang, Q. Fu and X. Bao, In situ identification of the metallic state of Ag nanoclusters in oxidative dispersion, *Nat. Commun.*, 2021, **12**, 1406.

38 C. Dong, R. Li, Z. Qu, Y. Fan, J. Wang, X. Du, C. Liu, X. Feng, Y. Ning, R. Mu, Q. Fu and X. Bao, Oxide Support Inert in Its Interaction with Metal but Active in Its Interaction with Oxide and Vice Versa, *J. Am. Chem. Soc.*, 2025, **147**, 13210–13219.

39 J. Soria, J. Sanz, I. Sobrados, J. M. Coronado, A. J. Maira, M. D. Hernández-Alonso and F. Fresno, FTIR and NMR Study of the Adsorbed Water on Nanocrystalline Anatase, *J. Phys. Chem. C*, 2007, **111**, 10590–10596.

40 L. Yang, M. Huang, N. Feng, M. Wang, J. Xu, Y. Jiang, D. Ma and F. Deng, Unraveling the atomic structure and dissociation of interfacial water on anatase $TiO_2(101)$ under ambient conditions with solid-state NMR spectroscopy, *Chem. Sci.*, 2024, **15**, 11902–11911.

41 K. Oka, T. Shibue, N. Sugimura, Y. Watabe, B. Winther-Jensen and H. Nishide, Long-lived water clusters in hydrophobic solvents investigated by standard NMR techniques, *Sci. Rep.*, 2019, **9**, 223.

42 S. M. Rau, R. J. Hirsch, M. Junige, A. S. Cavanagh, A. L. P. Rotondaro, H. Paddubrouskaya, K. H. Abel and S. M. George, Strongly and Weakly Adsorbed H_2O Layer Thicknesses on Hydroxylated SiO_2 Surfaces versus H_2O Pressure at Various Substrate Temperatures, *J. Phys. Chem. C*, 2025, **129**, 1666–1677.

43 H. Li, M. Abdelgaid, J. R. Paudel, N. P. Holzapfel, V. Augustyn, J. R. McKone, G. Mpourmpakis and E. J. Crumlin, Operando Unveiling of Hydrogen Spillover Mechanisms on Tungsten Oxide Surfaces, *J. Am. Chem. Soc.*, 2025, **147**, 6472–6479.

44 D. B. Asay and S. H. Kim, Evolution of the Adsorbed Water Layer Structure on Silicon Oxide at Room Temperature, *J. Phys. Chem. B*, 2005, **109**, 16760–16763.

45 A. Y. Nosaka, T. Fujiwara, H. Yagi, H. Akutsu and Y. Nosaka, Characteristics of Water Adsorbed on TiO_2 Photocatalytic Systems with Increasing Temperature as Studied by Solid-State ^1H NMR Spectroscopy, *J. Phys. Chem. B*, 2004, **108**, 9121–9125.

46 F. Kraushofer, L. Haager, M. Eder, A. Rafsanjani-Abbasi, Z. Jakub, G. Franceschi, M. Riva, M. Meier, M. Schmid, U. Diebold and G. S. Parkinson, Single Rh adatoms stabilized on $\alpha\text{-}Fe_2O_3(1\text{-}102)$ by coadsorbed water, *ACS Energy Lett.*, 2022, **7**, 375–380.

47 R. D. Glover, J. M. Miller and J. E. Hutchison, Generation of metal nanoparticles from silver and copper objects: nanoparticle dynamics on surfaces and potential sources

of nanoparticles in the environment, *ACS Nano*, 2011, **5**, 8950–8957.

48 A. Y. Nosaka, E. Kojima, T. Fujiwara, H. Yagi, H. Akutsu and Y. Nosaka, Photoinduced Changes of Adsorbed Water on a TiO_2 Photocatalytic Film As Studied by ^1H NMR Spectroscopy, *J. Phys. Chem. B*, 2003, **107**, 12042–12044.

49 D. Y. Ong, Z. Yen, A. Yoshii, J. Revillo Imbernon, R. Takita and S. Chiba, Controlled Reduction of Carboxamides to Alcohols or Amines by Zinc Hydrides, *Angew. Chem.*, 2019, **131**, 5046–5051.

50 F. Ritter, T. P. Spaniol, I. Douair, L. Maron and J. Okuda, Molecular Zinc Hydride Cations $[ZnH]^+$: Synthesis, Structure, and CO_2 Hydrosilylation Catalysis, *Angew. Chem., Int. Ed.*, 2020, **59**, 23335–23342.

51 M. Tüchler, L. Gärtner, S. Fischer, A. D. Boese, F. Belaj and N. C. Mösch-Zanetti, Efficient CO_2 Insertion and Reduction Catalyzed by a Terminal Zinc Hydride Complex, *Angew. Chem.*, 2018, **130**, 7022–7025.

52 F. Ritter, L. J. Morris, K. N. McCabe, T. P. Spaniol, L. Maron and J. Okuda, Deaggregation of Zinc Dihydride by Lewis Acids Including Carbon Dioxide in the Presence of Nitrogen Donors, *Inorg. Chem.*, 2021, **60**, 15583–15592.

53 J. Szanyi, J. H. Kwak, R. J. Chimentao and C. H. F. Peden, Effect of H_2O on the Adsorption of NO_2 on γ-Al_2O_3: an in Situ FTIR/MS Study, *J. Phys. Chem. C*, 2007, **111**, 2661–2669.

54 S. Benkoula, O. Sublemontier, M. Patanen, C. Nicolas, F. Sirotti, A. Naitabdi, F. Gaie-Levrel, E. Antonsson, D. Aureau, F.-X. Ouf, S.-I. Wada, A. Etcheberry, K. Ueda and C. Miron, Water adsorption on TiO_2 surfaces probed by soft X-ray spectroscopies: bulk materials vs. isolated nanoparticles, *Sci. Rep.*, 2015, **5**, 15088.

55 A. Braun, F. Aksoy Akgul, Q. Chen, S. Erat, T.-W. Huang, N. Jabeen, Z. Liu, B. S. Mun, S. S. Mao and X. Zhang, Observation of Substrate Orientation-Dependent Oxygen Defect Filling in Thin $WO_{3-\delta}/TiO_2$ Pulsed Laser-Deposited Films with in Situ XPS at High Oxygen Pressure and Temperature, *Chem. Mater.*, 2012, **24**, 3473–3480.

56 H. Zhang, H. Sun, D. Zhang, W. Zhang, S. Chen, M. Li and P. Liang, Nanoconfinement of Ag nanoparticles inside mesoporous channels of MCM-41 molecule sieve as a regenerable and H_2O resistance sorbent for Hg^0 removal in natural gas, *Chem. Eng. J.*, 2019, **361**, 139–147.

57 W. Yu, X. Yu and S.-T. Tu, Oxidation of Hydrogen Off-gas from a Fuel Cell Using a Microstructured Reactor with Hydrophobic Pt-Al_2O_3 Catalyst Coating, *Energy Procedia*, 2014, **61**, 2854–2857.

58 Y. Xu, X. Li, J. Gao, J. Wang, G. Ma, X. Wen, Y. Yang, Y. Li and M. Ding, A hydrophobic FeMn@Si catalyst increases olefins from syngas by suppressing C1 by-products, *Science*, 2021, **371**, 610–613.

59 C. Chen, M. Sun, Z. Hu, J. Ren, S. Zhang and Z.-Y. Yuan, New insight into the enhanced catalytic performance of ZnPt/HZSM-5 catalysts for direct dehydrogenation of propane to propylene, *Catal. Sci. Technol.*, 2019, **9**, 1979–1988.

60 S. M. T. Almutairi, B. Mezari, P. C. M. M. Magusin, E. A. Pidko and E. J. M. Hensen, Structure and Reactivity of Zn-Modified ZSM-5 Zeolites: The Importance of Clustered Cationic Zn Complexes, *ACS Catal.*, 2011, **2**, 71–83.

61 T. Gong, L. Qin, J. Lu and H. Feng, ZnO modified ZSM-5 and Y zeolites fabricated by atomic layer deposition for propane conversion, *Phys. Chem. Chem. Phys.*, 2016, **18**, 601–614.

62 C. Chen, Z. Hu, J. Ren, S. Zhang, Z. Wang and Z.-Y. Yuan, ZnO Nanoclusters Supported on Dealuminated Zeolite β as a Novel Catalyst for Direct Dehydrogenation of Propane to Propylene, *ChemCatChem*, 2019, **11**, 868–877.

63 C. Chen, Z.-P. Hu, J.-T. Ren, S. Zhang, Z. Wang and Z.-Y. Yuan, ZnO supported on high-silica HZSM-5 as efficient catalysts for direct dehydrogenation of propane to propylene, *Mol. Catal.*, 2019, **476**, 110508.

64 G. Liu, L. Zeng, Z.-J. Zhao, H. Tian, T. Wu and J. Gong, Platinum-Modified ZnO/Al_2O_3 for Propane Dehydrogenation: Minimized Platinum Usage and Improved Catalytic Stability, *ACS Catal.*, 2016, **6**, 2158–2162.

65 F. Zhang, C. Miao, Y. Yue, W. Hua and Z. Gao, Dehydrogenation of Propane to Propylene in the Presence of CO_2 over Steaming-treated HZSM-5 Supported ZnO, *Chin. J. Chem.*, 2012, **30**, 929–934.

66 Y. Chai, S. Chen, Y. Chen, F. Wei, L. Cao, J. Lin, L. Li, X. Liu, S. Lin, X. Wang and T. Zhang, Dual-Atom Catalyst with N-Colligated Zn_1Co_1 Species as Dominant Active Sites for Propane Dehydrogenation, *J. Am. Chem. Soc.*, 2024, **146**, 263–273.